J Electr Eng Technol.2017; 12(6): 2289-2297
http://doi.org/10.5370/JEET.2017.12.6.2289

ISSN(Print) 1975-0102
ISSN(Online) 2093-7423

PIR Speed Control Method of AC Motors Considering Time Delay in Speed Information

Jung-Ho Lee* and Jong-Woo Choi†

Abstract – Applying a periodic load torque to an AC motor generates a ripple, which is synchronized to the frequency of the periodic load torque, at the speed of the motor. Consequently, numerous studies have focused on reducing the speed ripple caused by the load torque. However, it is difficult to reduce the speed ripple when there is a time delay in acquiring speed information, such as that from a sensorless control. Therefore, we propose a speed control method for reducing speed ripples caused by a periodic load torque when there is a time delay in acquiring the speed information. The proposed method is verified by conducting simulations using the Simulink program from MATLAB, and by applying the method to an actual motor in which speed ripples occur due to a periodic load torque that is synchronized with the speed of the motor.

Keywords: Proportional-integral-resonant controller, Torque ripple, Speed ripple, Time delay, All-pass filter

1. Introduction

AC motors have found utility over a wide application range from industrial products to household appliances. As their fields of application are various, the types of loads they handle also become diverse. In the motor driving system, if a ripple occurs in the torque due to an applied load, a ripple is also generated in the speed. Other reasons for torque ripple to occur in motor driving systems include current offset, current scaling error, rotor eccentricity, current distortion due to dead-time, and periodic load torque. A speed ripple causes noise and vibration in the motor and degrades the control performance of the system. In particular, since household appliances are required to comply with certain standards of noise and vibration, it is important to suitably control and reduce torque ripples, i.e., speed ripples, in such systems [1].

Fig. 1 shows the load torque of a rolling-piston-type compressor that is commonly used in the outdoor unit of a low-power air-conditioning system. During the first half of the cycle (compression), as the pressure of the cylinder increases during the process of compressing the refrigerant, the load torque of the motor also increases. In the second half of the cycle (discharge), during the process of discharging the refrigerant, the load torque of motor decreases. Therefore, the load torque fluctuates in periodic synchrony with the mechanical speed of the motor.

Vector control with precise torque control performance is widely used in the high-performance drives of AC motors. Performing the vector control operation requires relatively accurate data on the motor parameters. In addition, a rotor position detector or a speed detector is particularly required to determine the position of the flux [2-4]. However, the use of a speed or position detector may increase costs and also lead to many technical problems; the hardware becomes increasingly complex and the motor axial length has to be increased. In addition, it is very difficult to use the speed or position detector in harsh environments. Further, the speed or position detector and its cables require maintenance. Lastly, such a detector may form the source of electrical noise. In order to resolve such problems, numerous studies have focused on sensorless control, i.e., control without the use of a speed or position detector. However, due to the characteristics of sensorless control, the speed control system exhibits a time delay in acquiring the speed information [5-10].

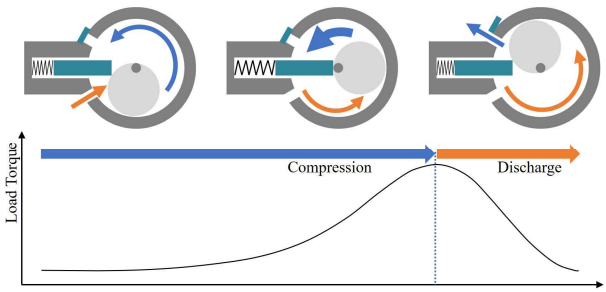

Fig. 1. Load torque of rolling-piston-type compressor

Against this backdrop, this study proposes a speed control method that reduces the speed ripple generated by the torque ripple in case of a time delay in acquiring speed information. When a load torque synchronized with the mechanical rotation angle is applied to the motor driving system, then the load torque periodically changes with rotation of the motor, and a synchronized speed ripple

† Corresponding Author: Dept. of Electrical Engineering, Kyungpook National University, Daegu, Korea. (cjw@knu.ac.kr)
* Dept. of Electrical Engineering, Kyungpook National University, Daegu, Korea. (mnljh20000@naver.com)
Received: May 12, 2017; Accepted: August 7, 2017

eventually occurs. A promising method for reducing the speed ripple caused by a periodic load torque is the proportional-integral-resonance (PIR) speed controller. However, when there is a delay in speed-information acquisition, the torque command exhibits a phase difference with the actual torque ripple. Thus, a satisfactory compensation result cannot be obtained [11, 12].

In order to solve this issue, our proposed speed controller utilizes an all-pass filter to compensate for the time delay in the PIR speed controller. We use the Nyquist criterion in order to analyze the stability of the speed control system based on the proposed speed controller [13, 14]. The performance of the proposed controller is compared with those of both an existing proportional-integral (PI) speed controller and PIR speed controller through simulations and experiments.

2. Existing Speed Controllers

2.1 Speed control system based on pi speed controller

Fig. 2 shows a speed control system based on a PI controller. Because the response of the current controller is significantly faster than that of the speed controller, we may assume that the transfer function of the current controller is unity. The transfer function between the actual speed and reference speed is expressed as (1), and the transfer function between the speed and load torque is expressed as (2) where K_T, J, K_{ps}, and K_{is} represent the torque constant, inertia of the motor, proportional gain, and integral gain, respectively.

When the load torque is constant, the speed response due to the load torque becomes zero in a steady state, and therefore, the speed response fully "follows" the system command. However, if the load torque is not constant, then the speed response due to the load torque is not zero in the steady state, and the speed cannot be implemented as per the command. When a periodic load torque is applied, a speed ripple synchronized to the load torque occurs.

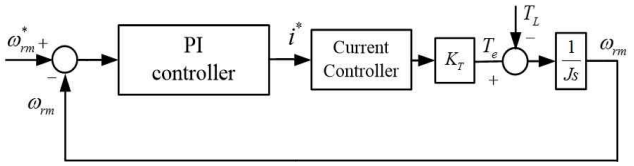

Fig. 2. Speed control system based on proportional-integral (PI) speed controller

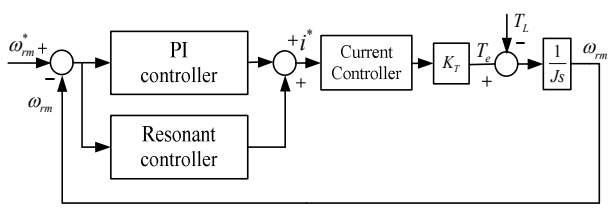

Fig. 3. Speed control system based on proportional-integral-resonant (PIR) speed controller

$$\frac{\omega_{rm}(s)}{\omega^*_{rm}(s)} = \frac{\frac{K_T K_{ps}}{J}s + \frac{K_T K_{is}}{J}}{s^2 + \frac{K_T K_{ps}}{J}s + \frac{K_T K_{is}}{J}} \tag{1}$$

$$\frac{\omega_{rm}(s)}{T_L(s)} = \frac{\frac{1}{J}s}{s^2 + \frac{K_T K_{ps}}{J}s + \frac{K_T K_{is}}{J}} \tag{2}$$

2.2 Speed control system based on pir speed controller

Fig. 3 shows the speed control system based on a PIR controller. A PIR controller includes a resonant controller that is connected in parallel with the PI controller. In this approach, the PI controller is the main controller that controls the DC component of the speed command, and the ripple component caused by the load torque (disturbance) that is not compensated by the main controller is controlled through the resonant controller. Assuming that the current control system is ideal, the transfer function between the actual speed and reference speed with the PIR speed controller is expressed as in (3), and the transfer function between the speed and load torque is expressed as in (4). In the equations below, K_{rs} denotes the resonant gain and ω_0 the resonant frequency.

$$\frac{\omega_{rm}(s)}{\omega^*_{rm}(s)} = \frac{\left(K_{ps} + \frac{K_{is}}{s} + \frac{K_{rs}s}{s^2+\omega_0^2}\right)\frac{K_T}{Js}}{1 + \left(K_{ps} + \frac{K_{is}}{s} + \frac{K_{rs}s}{s^2+\omega_0^2}\right)\frac{K_T}{Js}} \tag{3}$$

$$\frac{\omega_{rm}(s)}{T_L(s)} = \frac{\frac{1}{Js}}{1 + \left(K_{ps} + \frac{K_{is}}{s} + \frac{K_{rs}s}{s^2+\omega_0^2}\right)\frac{K_T}{Js}} \tag{4}$$

A PIR speed controller controls the DC component of the speed command using the PI controller and the ripple component caused by the load torque using the resonant controller. Because the resonant controller has a phase delay of 0° and infinite gain at resonant frequency, it can suitably generate torque commands of the ripple component caused by the load torque. In a speed control system based on a PIR controller, the speed response due to the reference speed at the resonant frequency is "1," and the speed response due to the periodic load torque is "0"; therefore, the system can completely compensate for the speed ripple caused by a periodic load torque. However, using an existing PIR speed controller for a motor driving system with a time delay in speed-information acquisition results in the controller generating a torque command based on

incorrect speed information; therefore, it is difficult to fully compensate for the distorted values due to the phase difference with the actual torque ripple. When compensating for distorted values, the control performance of the entire system cannot be guaranteed, and this may result in an even greater speed ripple.

3. Proposed Speed Controller

3.1 Speed control system based on proposed speed controller

Fig. 4 shows the speed control system with the proposed speed controller. In our approach, to compensate for the time delay of speed-information acquisition in an existing PIR speed controller, a first-order all-pass filter is connected in series with the resonant controller. Eq. (5) expresses the transfer function of the first-order all-pass filter as below:

$$G_{APF}(s)=\frac{s-\omega_{APF}}{s+\omega_{APF}} \tag{5}$$

The all-pass filter only changes the phase without changing the magnitude of the output. As shown in Fig. 5 and expressed in (6), when ω_{APF} is set at an appropriate value in accordance with the input, an output with the desired phase shifts at a specific frequency can be obtained.

$$\theta_{APF}=\pi-2\tan^{-1}\left(\frac{\omega}{\omega_{APF}}\right) \tag{6}$$

Eq. (7) expresses the transfer function between the actual speed and reference speed of the speed control system based on the proposed speed controller, and (8) expresses the transfer function between the speed and the load torque.

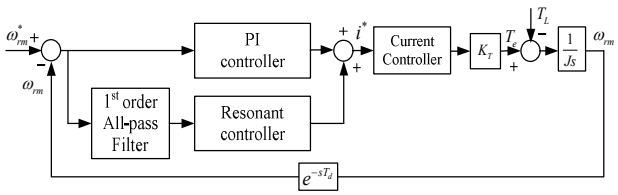

Fig. 4. Speed control system based on proposed speed controller

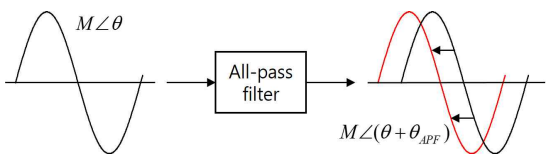

Fig. 5. Phase shift of all-pass filter

$$\frac{\omega_{rm}(s)}{\omega_{rm}^{*}(s)}=\frac{\left(K_{ps}+\frac{K_{is}}{s}+\frac{s-\omega_{APF}}{s+\omega_{APF}}\frac{K_{rs}s}{s^2+\omega_0^2}\right)\frac{K_T}{Js}}{1+e^{-sT_d}\left(K_{ps}+\frac{K_{is}}{s}+\frac{s-\omega_{APF}}{s+\omega_{APF}}\frac{K_{rs}s}{s^2+\omega_0^2}\right)\frac{K_T}{Js}} \tag{7}$$

$$\frac{\omega_{rm}(s)}{T_L(s)}=\frac{\frac{1}{Js}}{1+e^{-sT_d}\left(K_{ps}+\frac{K_{is}}{s}+\frac{s-\omega_{APF}}{s+\omega_{APF}}\frac{K_{rs}s}{s^2+\omega_0^2}\right)\frac{K_T}{Js}} \tag{8}$$

3.2 Nyquist criterion of time delay system

The Nyquist criterion is used to analyze the stability of a speed control system based on the proposed speed controller and to determine the range of ω_{APF}.

Assuming that the current control system is ideal and that there is no time delay in speed-information acquisition, the loop transfer function of the proposed speed control system is expressed as

$$L_1(s)=\left(K_{ps}+\frac{K_{is}}{s}+\frac{s-\omega_{APF}}{s+\omega_{APF}}\frac{K_{rs}s}{s^2+\omega_0^2}\right)\frac{K_T}{Js} \tag{9}$$

In order for the closed-loop system to be stable, the following equation must be satisfied:

$$\Phi_{11}=(Z-P-0.5P_{\omega})\cdot 180^{\circ} \tag{10}$$

Here, Φ_{11} denotes the total angle traversed by the phasor drawn from point $(-1, j0)$ to the Nyquist plot of $L_1(j\omega)$ as ω varies from infinity to zero. Further, Z represents the number of zeros corresponding to $1+L_1(s)$ in the right half plane, P the number of poles corresponding to $1+L_1(s)$ in the right half plane, and P_{ω} the number of poles of $1+L_1(s)$ on the $j\omega$-axis including the origin. In the proposed system, Z and P are "0" and P_{ω} is "4," and therefore, for the proposed system to be stable, Φ_{11} should be -360°.

The loop transfer function of the proposed system with time delay in speed-information acquisition is expressed as (11). Here, T_d indicates the delay time of the speed information.

$$L(s)=\left(K_{ps}+\frac{K_{is}}{s}+\frac{s-\omega_{APF}}{s+\omega_{APF}}\frac{K_{rs}s}{s^2+\omega_0^2}\right)\frac{K_T}{Js}e^{-T_d s} \tag{11}$$

The roots of the characteristic equation must satisfy (12) below:

$$\begin{aligned} q(s)&=1+L(s)\\ &=1+L_1(s)e^{-T_d s}\\ &=0 \end{aligned} \tag{12}$$

From the characteristic equation of (12), we derive (13) as

$$L_1(s) = -e^{T_d s} \tag{13}$$

Calculating (13) in the frequency domain, we have

$$\begin{aligned} L_1(j\omega) &= \left|L_1(j\omega)\right| \angle L_1(j\omega) \\ &= e^{j(\pi+\omega T_d)} \end{aligned} \tag{14}$$

Parameter $L_1(j\omega)$ in (14) signifies the Nyquist plot of the loop transfer function when there is no time delay in the system, and $e^{j(\pi+\omega T_d)}$ indicates a critical locus with a size of "1" and a phase of $\pi + \omega T_d$ rad. In other words, it expresses a critical locus that starts at point $(-1, j0)$ when the critical point is $\omega = 0$. As ω increases, the critical locus orbits along above the unit circle of radius "1" from the starting point in a counterclockwise direction.

The frequency that satisfies (15) is defined as ω_g, where ω_g denotes the gain-crossover frequency. The Nyquist plot of the loop transfer function excluding time delay $L_1(j\omega)$ intersects the critical locus at ω_g. Therefore, the Nyquist plot of the loop transfer function including time delay $L(j\omega)$ crosses the critical point $(-1, j0)$ at ω_g.

For a stable system, i.e., for $\Phi_{11} = -360°$, the Nyquist plot must lie to the right of the critical point so as to satisfy (16).

$$\left|L_1(j\omega)\right|_{\omega=\omega_g} = 1 \tag{15}$$

$$\angle L_1(j\omega_g) > \pi + \omega_g T_d \tag{16}$$

Parameter T_d can be obtained through calculation or measurement, and thus, the ω_{APF} range for the proposed system to be stable can be calculated as follows.

From (14), $L_1(j\omega)$ can be expressed as

$$L_1(j\omega) = Me^{j\theta} \tag{17}$$

and $L(j\omega)$ can be derived from (9), (11), and (17) as

$$L(j\omega) = Me^{j(\theta-\omega T_d)} \tag{18}$$

The equation that the imaginary part of $L(j\omega)$ satisfies "0" is expressed as (19) below:

$$\theta(\omega, \omega_{APF}) - \omega T_d = 0 \text{ or } \pi \;\rightarrow\; f(\omega, \omega_{APF}) = 0 \tag{19}$$

Further, the equation that the magnitude of $L(j\omega)$ satisfies "1" is defined as (20) below:

$$M(\omega, \omega_{APF}) = 1 \;\rightarrow\; g(\omega, \omega_{APF}) = 0 \tag{20}$$

Eq. (21) can be derived from (19) and (20) as

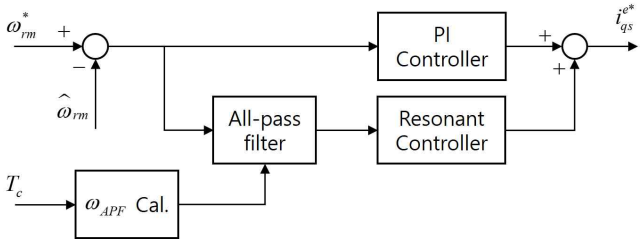

Fig. 6. Block diagram of proposed speed controller

$$\begin{aligned} \omega_{APF} &= f_1(\omega), f_2(\omega) \\ \omega_{APF} &= g_1(\omega), g_2(\omega) \end{aligned} \tag{21}$$

The maximum and minimum values of ω_{APF} correspond to the intersection of $g_1(\omega)$ and $f_1(\omega)$ or $f_2(\omega)$, or the intersection of $g_2(\omega)$ and $f_1(\omega)$ or $f_2(\omega)$.

Parameter ω_{APF} cannot be intuitively grasped, and the range of ω_{APF} varies greatly depending on the motor speed. Therefore, ω_{APF} is replaced with compensation time T_c, as in (22) below:

$$T_c = \frac{T_s}{2\pi}\left(\pi - \tan^{-1}\left(\frac{\omega_{rm}}{\omega_{APF}}\right)\right) \tag{22}$$

Fig. 6 shows the block diagram of the proposed speed controller. Parameter ω_{APF} can be calculated as per (23)

$$\omega_{APF} = \frac{\omega_{rm}}{\tan\left(\left|\frac{\pi}{2} - \frac{T_c}{T_s} \times \pi\right|\right)} \tag{23}$$

4. Simulation Results

The Nyquist criterion was applied to the proposed speed control method to determine stability and estimate the T_c range for the proposed system to be stable, and verification was performed through simulations using the Simulink program of MATLAB. The parameters and ratings of the induction motor used in the simulation are listed in Table 1.

The simulation was designed assuming that the pulse width modulator (PWM) inverter used in the control setup is ideal. In the discrete-time domain, the controls were set as follows: $100\mu s$ for the sampling times of the current controller, $400\mu s$ for the sampling times of the

Table 1. Induction motors specifications

Rated Power	1.5 kW
Number of Poles	4
Rated Current	5.5 A
Rated Speed	1435 rpm
Rated Frequency	50 Hz
Rated Torque	9.44 Nm
Motor Inertia	0.0054kgm^2

flux controller and speed controller. The speed and position information used for the controllers were obtained through sensorless control, and the speed error was measured using the actual motor speed.

Table 2. Simulation and experimental conditions

PI Flux Controller Bandwidth	30 rad/s
PI Speed Controller Bandwidth	100 rad/s
PI Current Controller Bandwidth	1500 rad/s
Resonant Controller Gain	30
Time Delay of Speed Information	4.5 ms
Compensation Time (T_c)	10 ms

Table 3. Range of compensation time (T_c)

ω_{rpm}^* [rpm]	T_{c_min} [ms]	T_{c_max} [ms]
300 rpm	0	8.57 ms
600 rpm	0	11.26 ms
900 rpm	2.29 ms	14.39 ms
1200 rpm	3.31 ms	16.84 ms
1500 rpm	3.52 ms	17.66 ms

The speed error of the speed control systems based on the PIR speed controller and the proposed speed controller were compared under the assumption that the time delay of the speed information was 4.5 ms. The simulation conditions are listed in Table 2.

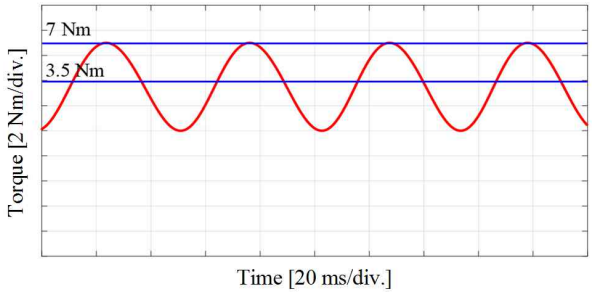

Fig. 7. Load torque ($\omega_{rpm}^* = 1200$ rpm)

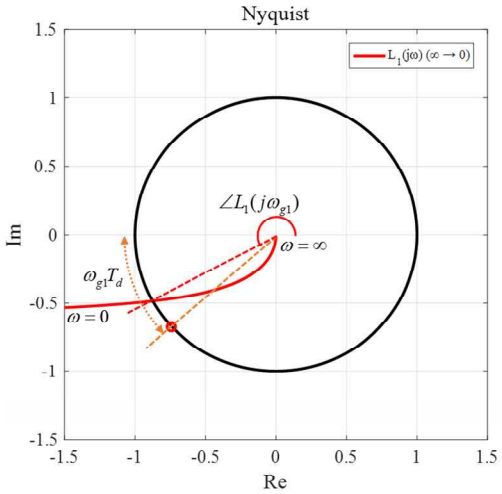

(a) $T_c = 0$ (unstable)

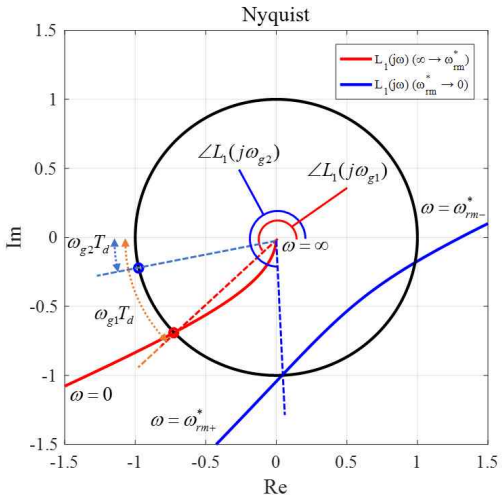

(b) $T_c = 3.31$ ms (critical)

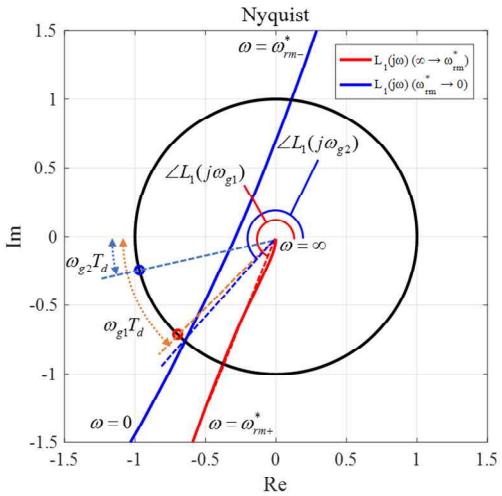

(c) $T_c = 10$ ms (stable)

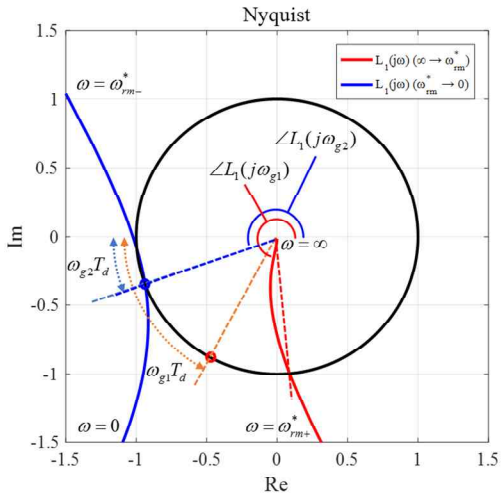

(d) $T_c = 16.84$ ms (critical)

Fig. 8. Nyquist plot of speed control system based on proposed speed controller for variation in T_c ($\omega_{rpm}^* = 1200$ rpm)

Fig. 7 depicts the load torque applied to the motor. The load torque of 7 Nm was applied in the form of a sine wave, and the torque was approximately 70 % of the motor rating and synchronized with the motor speed.

The T_c range for the proposed system to be stable was obtained by application of the Nyquist criterion, as listed in Table 3.

Fig. 8 shows the Nyquist plot according to the changes in T_c in the speed control system using the proposed speed controller at a reference speed of 1200 rpm. In Fig. 8, ω_{g1} and ω_{g2} represent the frequencies at which the Nyquist plot of $L(j\omega)$ passes the critical point $(-1, j0)$ when ω changes from infinity to ω^*_{rm+}, and when it changes from ω^*_{rm-} to zero, respectively. When $T_c = 0$, i.e., when the time delay is not compensated, the Nyquist plot of $L_1(j\omega)$ lies to the left of the critical point; therefore, the system becomes unstable. As shown in Fig. 8(b), increasing the value of T_c to 3.31 ms in order to compensate for the time delay results in the Nyquist plot of $L_1(j\omega)$ meeting the critical point corresponding to ω_{g1}. In addition, as shown in Fig. 8(c), if the value of T_c is set to be greater than 3.31 ms, then the Nyquist plot of $L_1(j\omega)$ lies to the right of the critical point, thereby indicating that the system is stable. On the other hand, continuously increasing the value of T_c to reach a final value of 16.84 ms results in the Nyquist plot of $L_1(j\omega)$ meeting the critical point of ω_{g2}, thus indicating that the system is unstable. In other words, the system is stable when the value of T_c is set between 3.31 and 16.84 ms for a reference speed of 1200 rpm. In the simulation, the compensation time T_c was set to 10 ms.

The initial part of the plot (corresponding to the PI controller) in Fig. 9 indicates the speed error of the speed control system based on the PI speed controller in which a synchronized speed ripple at a motor speed of approximately ±65 rpm was present.

From Fig. 9(a), we observe that the speed error increases when the PIR speed controller is used, which means that the system becomes unstable owing to the time delay in speed-information acquisition. Using a PIR speed controller in a motor-driven system with a time delay in the speed information leads to the entire system becoming unstable, and it may result in an even greater speed ripple than that obtained with a PI speed controller. Fig. 9(b) shows the speed error of the speed control system based on the proposed speed controller. The value of T_c corresponding to this case was 10 ms, and through the Nyquist criterion, the value was set within the range in which the system was stable. From the figure, we note that using the proposed speed controller results in the speed error converging to zero in the steady state.

Figs. 10 and 11 illustrate the speed error for reference speeds of 1200 rpm and 1500 rpm, respectively. These results indicate that periodic speed errors of ±55 rpm (Fig. 10) and ±45 rpm (Fig. 11) occurred when using the PI speed controller. Further, from the figures, we observe that the speed error increases when the PIR speed controller is used (Figs. 10(a) and 11(a)). On the other hand, when the proposed speed controller is used, a reduction in speed error of approximately ±10 rpm is observed (Figs. 10(b) and 11(b)). Thus, we confirmed that the use of the proposed speed controller yielded a superior performance in terms of speed ripple reduction when compared with that of an existing speed controller.

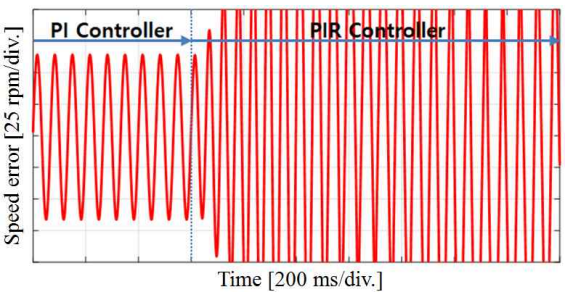

(a) Proportional-integral-resonance (PIR) speed controller

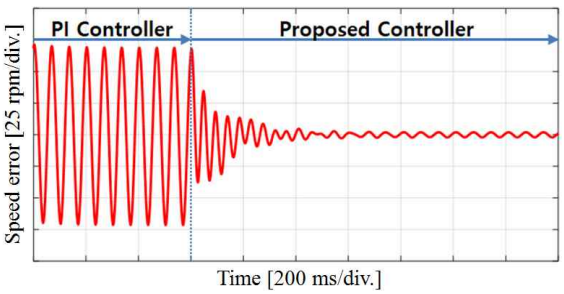

(b) Proposed speed controller

Fig. 9. Simulation results ($\omega^*_{rpm} = 900$ rpm)

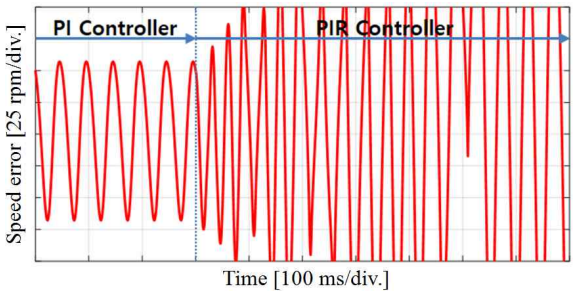

(a) Proportional-integral-resonance (PIR) speed controller

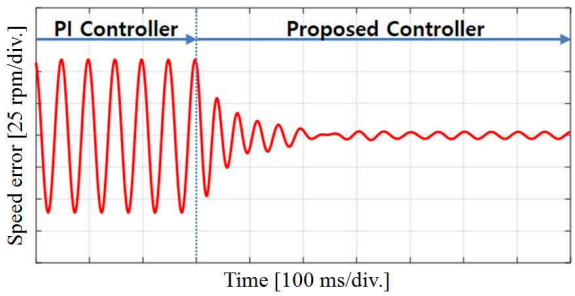

(b) Proposed speed controller

Fig. 10. Simulation results ($\omega^*_{rpm} = 1200$ rpm)

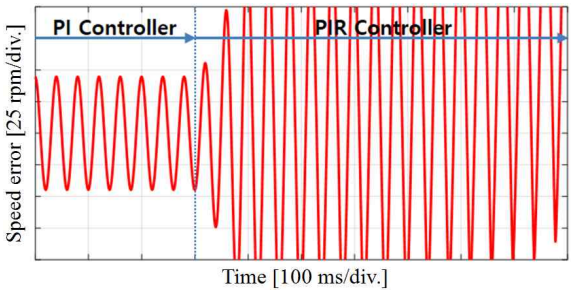

(a) PIR speed controller

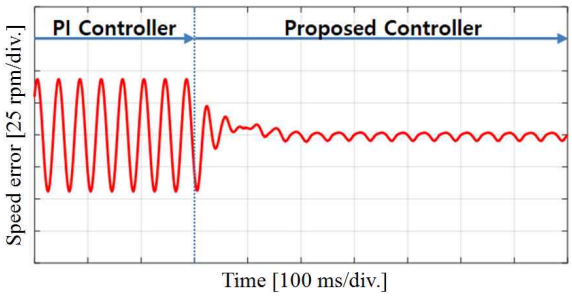

(b) Proposed speed controller

Fig. 11. Simulation results ($\omega_{rpm}^{*} = 1500$ rpm)

5. Experimental Results

We confirmed through simulations that the proposed speed controller method offers a superior performance in speed ripple reduction over the existing methods. This performance was verified by applying the method to an actual motor in which an actual periodic load torque synchronized with the motor speed was applied. The experimental set of the proposed speed control system is shown in Fig. 12. TMS320F28335 was employed as a digital signal processor (DSP) in the experiment, and a servo drive system was used to generate the load torque.

The motor rating used for experiments was same as that of the simulation, and the experimental conditions were also consistent with the simulation. The motor was driven by a sensorless vector control, and the time delay in speed-information acquisition was about 4.5 ms. As in the simulation, we compared the speed errors of the speed control systems to which the PI speed controller, the PIR speed controller, and the proposed speed controller were applied.

Fig. 13 depicts the speed error occurring in the actual motor with the application of a reference speed of 900 rpm. We note that the synchronized speed error obtained with the PI speed controller is approximately ±65 rpm.

From Fig. 13(a), we note that speed error increases when the PIR speed controller is used. This result indicates that the system becomes unstable owing to the time delay in acquiring the speed information.

Fig. 13(b) shows the speed error of the speed control system using proposed speed controller; the speed error is

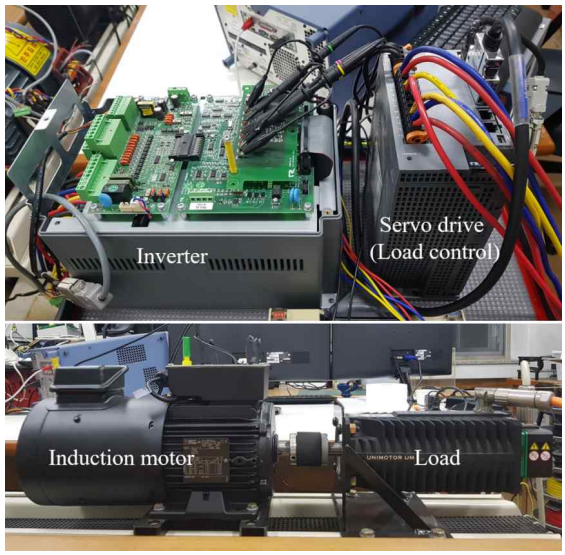

Fig. 12. Experimental set

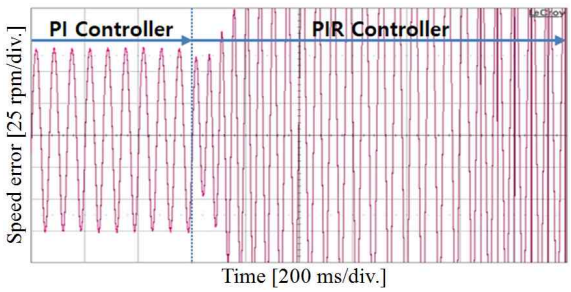

(a) Proportional-integral-resonance (PIR) speed controller

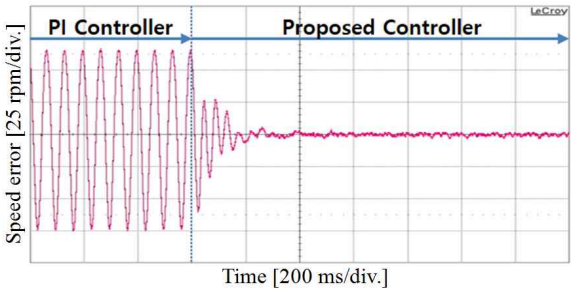

(b) Proposed speed controller

Fig. 13. Experimental results ($\omega_{rpm}^{*} = 900$ rpm)

reduced to nearly zero.

Figs. 14 and 15 show the speed errors corresponding to reference speeds of 1200 rpm and 1500 rpm, respectively. Periodic speed errors of −60 to +55 rpm (Fig. 13) and −40 to +45 rpm (Fig. 14) are observed when using the PI speed controller. Further, we note that the speed error increases when the PIR speed controller is used. On the other hand, with the proposed speed controller, a reduction to approximately ±10 rpm in the speed error is observed. Thus, we confirmed that the use of the proposed speed controller yields a superior performance in speed ripple reduction over that of an existing speed controller.

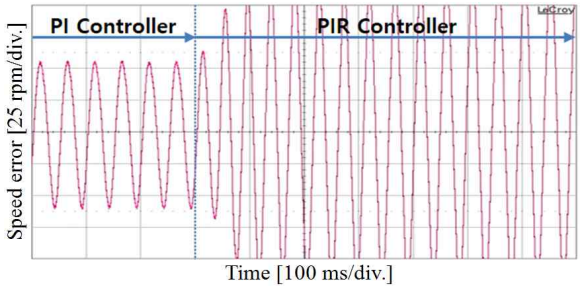

(a) Proportional-integral-resonance (PIR) speed controller

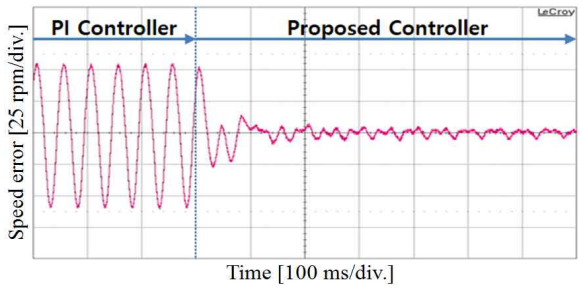

(b) Proposed speed controller

Fig. 14. Experimental results ($\omega^*_{rpm} = 1200$ rpm)

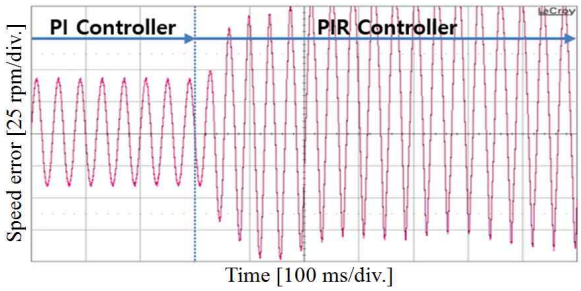

(a) Proportional-integral-resonance (PIR) speed controller

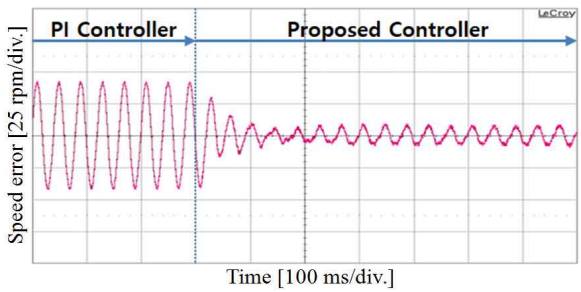

(b) Proposed speed controller

Fig. 15. Experimental results ($\omega^*_{rpm} = 1500$ rpm)

6. Conclusion

In this study, we proposed a speed control method for motor-driven systems with time delays in the acquisition of speed information. The proposed method reduces the periodic speed ripples caused by a periodic load torque according to the rotation of the motor. Through application of the Nyquist criterion, the proposed speed control method ensures system stability in the motor driving system with time delays in speed-information acquisition. Furthermore, the validity of the proposed speed control method was verified through simulations and experiments.

Acknowledgements

This work was supported by the Korea Institute of Energy Technology Evaluation and Planning (KETEP) and the Ministry of Trade, Industry & Energy (MOTIE) of the Republic of Korea (no. 20174030201490).

References

[1] K. Kenzo, O. Tsutomu and S. Takashi, "Application trends in AC motor drives," *IEEE IECON Conf. Rec.*, pp. 31-36, 1992.

[2] W. Leonhard, *Control of electrical drives,* 2nd ed., Springer, 1996.

[3] D. W. Novotny and etc., *Vector control and dynamics of AC drives*, Clarendon Press, Oxford, 1998.

[4] F. Briz and etc, "Speed measurement using rotary encoders for high performance AC drives," *IEEE IECON '94,* vol. 1, pp. 528-542, 1994.

[5] T. Ohtani and etc, "Vector control of induction motor without shaft encoder," *IEEE Trans. Industry Applications,* vol. 28, no. 1, pp. 157-164, Jan./Feb., 1992.

[6] T. Kume, et al., "High speed vector control without encoder for a high speed spindle motor," *IEEE IAS Conf. Rec*., pp. 390-394, 1990.

[7] K. Sakamoto, Y. Iwaji, T. Endo and Y. Takakura, "Position and speed sensorless control for PMSM drive using direct position error estimation," *IEEE IECON Conf. Rec*., pp. 1680-1685, 2001.

[8] Z. Chen, M. Tomita, S. Ichikawa, S. Doki and S. Okuma, "Sensorless control of interior permanent magnet synchronous motor by estimation of an extended electromotive force," *IEEE IAS Conf. Rec.,* vol. 3, pp. 1814-1819, Oct. 2000.

[9] Y. C. Son, B. H. Bae and S. K. Sul, "Sensorless operation of permanent magnet motor using direct voltage sensing circuit," *IEEE IAS Conf. Rec*., pp. 1674-1678, 2002.

[10] H. Kim and etc., "A New Motor Speed Estimator Using Kalman Filter in Low-Speed Range," *IEEE Transaction on Industry Application*, vol. 43, no. 4, pp. 701-705, August, 1991.

[11] S. Fukuda, T. yoda "A Novel Current-Tracking Method for Active Filters based on a Sinusoidal Internal Model," *IEEE Trans. Industry Applications*, vol. 37, no. 3, pp. 888-895, May/June. 2001.

[12] Changliang Xia and etc., "Smooth Speed Control

for Low-Speed High-Torque Permanent-Magnet Synchronous Motor Using Proportional-Integral-Resonant Controller," *IEEE Trans. Industrial Electronics*, vol. 62, no. 4, April, 2015.
[13] G. Franklin and etc., *Feedback Control of Dynamic System*, 2nd ed., Addison-Weseley, pp. 361-458, 1991.
[14] Benjamin C. Kuo, *Automatic Control Systems*, 2nd ed., Prentice Hall, 2009.

Jung-Ho Lee received B.S. and M.S. degrees in electrical engineering from Kyungpook National University, Daegu, Korea, in 2012 and 2014, respectively, and is currently working toward his Ph.D. degree in electrical engineering at Kyungpook National University. His currently research interests include power-electronic control of electric machines and custom power devices.

Jong-Woo Choi received B.S., M.S., and Ph.D. degrees in electrical engineering from Seoul National University, Seoul, Korea, in 1991, 1993, and 1996, respectively. He worked as a research engineer at LG Industrial Systems Company from 1996 to 2000. Since 2001, he has been a faculty member of the Department of Electrical Engineering, Kyungpook National University, Daegu, Korea, where he is currently a professor. His current research interests include static power conversion and electric machine drives.